Analytical solutions of transient pulsed eddy current problem due to elliptical electromagnetic concentrative coils*

Xiao Chun-Yan(肖春燕)† and Zhang Jun(张 军)

Department of Electrical Engineering, School of Automation and Electrical Engineering, Beihang University, Beijing 100191, *China*

(Received 19 March 2010; revised manuscript received 9 July 2010)

The electromagnetic concentrative coils are indispensable in the functional magnetic stimulation and have potential applications in nondestructive testing. In this paper, we propose a figure-8-shaped coil being composed of two arbitrary oblique elliptical coils, which can change the electromagnetic concentrative region and the magnitude of eddy current density by changing the elliptical shape and/or spread angle between two elliptical coils. Pulsed current is usually the excitation source in the functional magnetic stimulation, so in this paper we derive the analytical solutions of transient pulsed eddy current field in the time domain due to the elliptical concentrative coil placed in an arbitrary position over a half-infinite plane conductor by making use of the scale-transformation, the Laplace transform and the Fourier transform are used in our derivation. Calculation results of field distributions produced by the figure-8-shaped elliptical coil show some behaviours as follows: 1) the eddy currents are focused on the conductor under the geometric symmetric centre of figure-8-shaped coil; 2) the greater the scale factor of ellipse is, the higher the eddy current density is and the wider the concentrative area of eddy current along y axis is; 3) the maximum magnitude of eddy current density increases with the increase of spread angle. When spread angle is 180°, there are two additional reverse concentrative areas on both sides of x axis.

Keywords: transient pulsed eddy current, analytical solution, elliptical electromagnetic concentrative coil, functional magnetic stimulation

PACC: 0350D, 8760D, 8170C, 0200

1. Introduction

The electromagnetic concentrative coils are initially used for functional magnetic stimulation in order to induce currents only in the target biological tissue and avoid the undesirable side effects. At present, electromagnetic concentrative coils are required to induce very high current intensities in the specified deep region with lower frequency and good concentrative property in many applications, such as functional magnetic stimulation, bio-conductivity imaging,[1] pulsed eddy current nondestructive testing, etc.

There were several types of electromagnetic concentrative coils until now. Ueno *et al.*[2] employed a pair of oppositely connected coils in the functional magnetic stimulation in 1988, which was later developed into a more concentrative figure-8-shaped coil made of two oblique coils.[3] On this basis, many kinds of coils were designed for various applications, such as Slinky coils,[4] 3-D differential coils,[5] figure-B-shaped coils,[6] plane butterfly coils, plane 4-leaf coils, array coils, etc.[7−10] The problem of eddy current field produced by these coils at a given pulsed current is indispensable for functional magnetic stimulation. It is difficult to solve the analytical solution of the transient pulsed eddy current field produced by oblique electromagnetic concentrative coils, while it is a basic work. Tsaknakis and Kriezis[11] have given the eddy current distributions within a conducting plate produced by a circular current loop with pulsed current parallel or perpendicular to the plate, and they have also given the field distributions due to a circular current loop placed in an arbitrary position above a conducting plate and analytical solution of time-harmonic eddy current field.[12] Zhang and Lei[3] have given the analytical solution of time-harmonic eddy current field due to a figure-8-shaped coil composed by two oblique

*Project supported by the National Natural Science Foundation of China (Grant No. 50807001).

†Corresponding author. E-mail: xiao_chunyan@163.com or xiao_chunyan@buaa.edu.cn

© 2010 Chinese Physical Society and IOP Publishing Ltd

circular loop coils. Xie and Lei [13] have researched the time-varying linear electromagnetic initial-boundary value problem.

Based on the above research, the figure-8-shaped coil made of two arbitrary oblique elliptical coils is proposed in this paper, which can change the electromagnetic concentrative region and the magnitude of eddy current density by changing the elliptical shape and spread angle between two elliptical coils. Analytical solutions of transient pulsed eddy current due to elliptical concentrative coil placed in an arbitrary position over a half-infinite plane conductor are derived. First, the electromagnetic model of single elliptical coil placed in an arbitrary position over a half-infinite plane conductor is built, and the initial-boundary value problem is provided. Secondly, the electromagnetic field produced by an elliptical coil is solved by transforming it into a circular current loop by the scale-transformation, and the analytical solution of transient pulsed eddy current field produced by oblique elliptical coil in the s domain is obtained by making use of the Laplace transform, the Fourier transform and the inverse Fourier transform. Thirdly, the analytical solution in the time domain is obtained by the inverse scale-transformation and the inverse Laplace transform. Finally, for the figure-8-shaped coil composed of two oblique elliptical coils, the analytical results are obtained and compared with the numerical solutions by using Ansoft software. The eddy current fields are computed and the effects of coil's parameters on concentrative characteristics are analysed.

2. Electromagnetic model of elliptical coil placed in an arbitrary position

The oblique elliptical coil is neither parallel nor perpendicular to the surface of conductor with elliptical section. Figure 1 shows the coordinate system o-xyz and the electromagnetic model, where an oblique elliptical current loop C, made of thin wire, is located over a half-infinite plane conductor. Suppose the radius of transverse axis of elliptical coil is R, the longitudinal axis is parallel to y axis, and its radius ratio of longitudinal axis to transverse axis is η, called the scale factor. Axis z is through the geometric centre of elliptical coil. α is the angle between the normal direction of coil's plane and the positive direction of axis z, which is named the tilt angle of the coil. h is the distance from the geometric centre of coil to the plane xoy. The relationship between the reference direction of the current $i(t)$ in the coil and the positive direction of axis z obeys the right-hand screw relationship. The region 1, $z > 0$, is the air, $\mu_1 = \mu_0$ and $\sigma_1 = 0$; the region 2, $z < 0$, is the conductor, $\mu_2 = \mu = \mu_r\mu_0$ and $\sigma_2 = \sigma$. Suppose that the displacement current density is ignored.

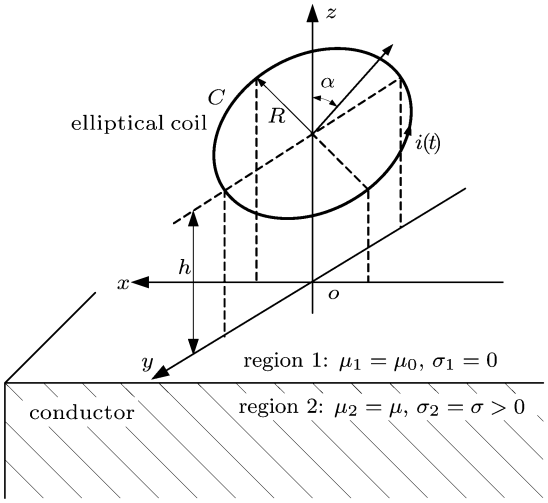


Fig. 1. Electromagnetic model of oblique elliptical coil.

Suppose that the waveform of the excitation current $i(t)$ is square wave, and the eddy currents at the end of each cycle decay to zero. We only calculate the field distributions produced by a single pulsed current, shown in Fig. 2. The expression of $i(t)$ is

$$i(t) = I_0[u(t) - u(t - t_0)], \tag{1}$$

where I_0 is the magnitude of electrical current and $u(t)$ is the unit step function,

$$u(t) = \begin{cases} 1, & t > 0, \\ 0, & t < 0. \end{cases}$$

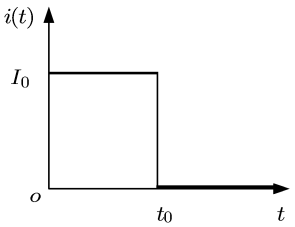


Fig. 2. The waveform of the exciting current.

Initial-boundary value problem of the electromagnetic field is written below.

(i) Equations

In the region 1, there is the exciting current density $\boldsymbol{J}$ and the electromagnetic fields satisfy

$$\boldsymbol{\nabla} \times \boldsymbol{H}_1 = \boldsymbol{J}, \tag{2}$$

$$\boldsymbol{\nabla} \times \boldsymbol{E}_1 = -\frac{\partial \boldsymbol{B}_1}{\partial t}. \tag{3}$$

In the region 2, there is the conduction current and the electromagnetic fields satisfy

$$\boldsymbol{\nabla} \times \boldsymbol{H}_2 = \sigma \boldsymbol{E}_2, \tag{4}$$

$$\boldsymbol{\nabla} \times \boldsymbol{E}_2 = -\frac{\partial \boldsymbol{B}_2}{\partial t}. \tag{5}$$

(ii) Initial conditions

$$\boldsymbol{E}_i|_{t\leq 0} = \boldsymbol{0}, \quad (i = 1,\ 2), \tag{6}$$

$$\boldsymbol{H}_i|_{t\leq 0} = \boldsymbol{0}, \quad (i = 1,\ 2). \tag{7}$$

(iii) Interface conditions

$$\boldsymbol{n}_{12} \times (\boldsymbol{H}_2 - \boldsymbol{H}_1) = \boldsymbol{0}, \quad (z = 0), \tag{8}$$

$$\boldsymbol{n}_{12} \times (\boldsymbol{E}_2 - \boldsymbol{E}_1) = \boldsymbol{0}, \quad (z = 0), \tag{9}$$

where $\boldsymbol{n}_{12}$ is the unit normal vector pointing from medium 1 to medium 2.

(iv) Finite conditions

$$\lim_{r\to\infty} r\boldsymbol{H}_i = \boldsymbol{D}_{i,h}\ , \quad (i = 1,\ 2), \tag{10}$$

$$\lim_{r\to\infty} r\boldsymbol{E}_i = \boldsymbol{D}_{i,e}, \quad (i = 1,\ 2), \tag{11}$$

where r is the size of field point's radius vector, $\boldsymbol{D}_{i,h}$ and $\boldsymbol{D}_{i,e}$ are all finite known vector.

3. Analytical solutions of transient pulsed eddy current problem due to the oblique elliptical coil

3.1. Magnetic vector potential in the conductor region

The region 2 is the conductor. Let $\boldsymbol{B} = \boldsymbol{\nabla} \times \boldsymbol{A}$. Substituting $\boldsymbol{H}_2 = \mu_2^{-1}\boldsymbol{\nabla} \times \boldsymbol{A}_2$ into Eq. (4) and according to the Coulomb's gauge

$$\boldsymbol{\nabla} \cdot \boldsymbol{A}_2 = 0, \tag{12}$$

the magnetic vector potential $\boldsymbol{A}_2$ in the region 2 produced by the eddy current satisfies the equation

$$\boldsymbol{\nabla}^2 \boldsymbol{A}_2 = \mu_2\sigma_2 \frac{\mathrm{d}\boldsymbol{A}_2}{\mathrm{d}t}.$$

Applying the Laplace transform to the above equation for the variable t,[14] then

$$\boldsymbol{\nabla}^2 \boldsymbol{A}_{2s} = \mu_2\sigma_2 s\boldsymbol{A}_{2s}, \tag{13}$$

where $\boldsymbol{A}_{2s}$ is the Laplace transform of $\boldsymbol{A}_2$. Applying the Fourier transforms[15] for the variables x, y and considering that the Fourier transform of $\boldsymbol{A}_{2s}(x, y, z)$ is $\boldsymbol{\alpha}_{2s}(u, v, z)$, equation (13) changes into

$$-u^2\boldsymbol{\alpha}_{2s} - v^2\boldsymbol{\alpha}_{2s} + \frac{\partial^2 \boldsymbol{\alpha}_{2s}}{\partial z^2} - \mu_2\sigma_2 s\boldsymbol{\alpha}_{2s} = \boldsymbol{0}. \tag{14}$$

Considering that the field distribution in the infinite space is finite, that is, Eqs. (10) and (11), the solution of Eq. (14) can be written as

$$\boldsymbol{\alpha}_{2s} = \boldsymbol{C}_{2s} 4\pi^2 \mathrm{e}^{\lambda z}, \tag{15}$$

where $\lambda = \sqrt{u^2 + v^2 + \mu_2\sigma_2 s}$, $\boldsymbol{C}_{2s}$ is the unknown coefficient in the s domain. Applying the inverse Fourier transform for the variables u and v, the expression (15) changes into

$$\boldsymbol{A}_{2s}(x, y, z, s) = \int_{-\infty}^{+\infty}\int_{-\infty}^{+\infty} \boldsymbol{C}_{2s}\mathrm{e}^{\lambda z + \mathrm{j}(ux+vy)}\mathrm{d}u\mathrm{d}v. \tag{16}$$

3.2. Magnetic vector potential in the air region

The magnetic vector potential $\boldsymbol{A}_1$ in the air region 1 is the sum of $\boldsymbol{A}_{11}$ produced by the elliptical coil and $\boldsymbol{A}_{12}$ produced by the eddy current in the conductor, that is

$$\boldsymbol{A}_1 = \boldsymbol{A}_{11} + \boldsymbol{A}_{12}. \tag{17}$$

3.2.1. Magnetic vector potential in the air region produced by the eddy current

Substituting $\boldsymbol{H}_1 = \mu_1^{-1}\boldsymbol{\nabla} \times \boldsymbol{A}_1$ into Eq. (2) and according to the Coulomb's gauge

$$\boldsymbol{\nabla} \cdot \boldsymbol{A}_1 = 0, \tag{18}$$

the magnetic vector potential $\boldsymbol{A}_{12}$ in the air region 1 produced by the eddy current satisfies the equation

$$\boldsymbol{\nabla}^2 \boldsymbol{A}_{12} = 0.$$

Applying the Laplace transform for the variable t for the above equation, then we have

$$\boldsymbol{\nabla}^2 \boldsymbol{A}_{12s} = \boldsymbol{0}, \tag{19}$$

where $\boldsymbol{A}_{12s}$ is the Laplace transform of $\boldsymbol{A}_{12}$. Applying the Fourier transforms for the variables x, y and considering that the Fourier transform of $\boldsymbol{A}_{12s}(x,y,z)$ is $\boldsymbol{\alpha}_{12s}(u,v,z)$, equation (19) changes into

$$-u^2\boldsymbol{\alpha}_{12s} - v^2\boldsymbol{\alpha}_{12s} + \frac{\partial^2\boldsymbol{\alpha}_{12s}}{\partial z^2} = \boldsymbol{0}. \tag{20}$$

Considering that the field distribution in the infinite space is finite, the solution of Eq. (20) can be written as

$$\boldsymbol{\alpha}_{12s} = \boldsymbol{C}_{1s}4\pi^2\mathrm{e}^{-kz}, \tag{21}$$

where $\boldsymbol{C}_{1s}$ is the unknown coefficient in the s domain. Applying the inverse Fourier transform for the variables u and v, the expression (21) changes into

$$\boldsymbol{A}_{12s}(x,y,z,s) = \int_{-\infty}^{+\infty}\int_{-\infty}^{+\infty}\boldsymbol{C}_{1s}\mathrm{e}^{-kz+\mathrm{j}(ux+vy)}\mathrm{d}u\mathrm{d}v. \tag{22}$$

3.2.2. Magnetic vector potential in the air region produced by the oblique elliptical coil

First, we give the expression of current density in the oblique elliptical coil.

The elliptical loop C can be expressed by the intersecting line of two surfaces

$$C:\begin{cases} m(x,y,z) = x\sin\alpha - (z-h)\cos\alpha = 0, \\ q(x,y,z) = \sqrt{[x\cos\alpha + (z-h)\sin\alpha]^2 + (y/\eta)^2} - R = 0, \end{cases} \tag{23}$$

where the equation $m(x,y,z)=0$ represents the plane of elliptical coil, and the equation $q(x,y,z)=0$ represents the oblique elliptical cylinder surface whose central axis is through the coil's geometric centre and perpendicular to the coil's plane.

For convenience, the scale-transformation[16] will be applied to transform the original coordinate system o–xyz into the new coordinate system o'–$x'y'z'$ in order to transform the elliptical current loop into the circular current loop. The relationship between two coordinates is that the origins of two coordinates coincide and

$$\boldsymbol{r}' = \boldsymbol{T}\cdot\boldsymbol{r}, \quad \boldsymbol{r} = [\,x\ y\ z\,]^{\mathrm{T}}, \quad \boldsymbol{r}' = [\,x'\ y'\ z'\,]^{\mathrm{T}}, \tag{24}$$

where the transformation matrix $\boldsymbol{T} = \begin{bmatrix} 1 & 0 & 0 \\ 0 & 1/\eta & 0 \\ 0 & 0 & 1 \end{bmatrix}$.

The expression of the circular loop C' in the new coordinates is

$$C':\begin{cases} m'(x',y',z') = x'\sin\alpha - (z'-h)\cos\alpha = 0, \\ q'(x',y',z') = \sqrt{[x'\cos\alpha + (z'-h)\sin\alpha]^2 + y'^2} - R = 0. \end{cases} \tag{25}$$

Then, the current density $\boldsymbol{J}'(x',y',z',t)$ at any point $P(x',y',z')$ in the coordinates o'–$x'y'z'$ in the region 1 can be expressed as

$$\begin{aligned} \boldsymbol{J}'(x',y',z',t) &= i(t)\delta(m')\delta(q')\frac{\nabla q'(P)\times\nabla m'(P)}{|\nabla q'(P)\times\nabla m'(P)|} \\ &= i(t)\delta(m')\delta(q')\frac{1}{\rho'}(-\boldsymbol{e}_{x'}y'\cos\alpha + \boldsymbol{e}_{y'}\chi' - \boldsymbol{e}_{z'}y'\sin\alpha), \end{aligned} \tag{26}$$

where $\chi' = x'\cos\alpha + (z'-h)\sin\alpha$ and $\rho' = \sqrt{\chi'^2 + y'^2}$.

After the scale-transformation, the magnetic vector potential $\boldsymbol{A}_{11}$ is transformed into

$$\boldsymbol{A}'_{11} = \boldsymbol{T}^{-1}\boldsymbol{A}_{11}, \tag{27}$$

and the electromagnetic parameters μ_1 and σ_1 are transformed into $\boldsymbol{\mu}'_1 = \mu_1\boldsymbol{M}^{-1}\boldsymbol{T}$ and $\boldsymbol{\sigma}'_1 = \sigma_1\boldsymbol{M}^{-1}\boldsymbol{T}$, where the transformation matrix $\boldsymbol{M} = \begin{bmatrix} 1/\eta & 0 & 0 \\ 0 & 1 & 0 \\ 0 & 0 & 1/\eta \end{bmatrix}$.

The magnetic vector potential $\boldsymbol{A}'_{11}$ in the air region produced by the coil satisfies

$$\boldsymbol{\nabla}' \times (\boldsymbol{\mu}'^{-1}_1 \boldsymbol{\nabla}' \times \boldsymbol{A}'_{11}) = \boldsymbol{J}'(P,t). \tag{28}$$

Applying the Laplace transform for the variable t to Eq. (28), we obtain

$$\begin{aligned} &\boldsymbol{\nabla}' \times (\boldsymbol{\mu}'^{-1}_1 \boldsymbol{\nabla}' \times \boldsymbol{A}'_{11s}) \\ &= I_s \delta(m')\delta(q')\frac{1}{\rho'}(-\boldsymbol{e}_{x'} y' \cos\alpha \\ &\quad + \boldsymbol{e}_{y'}\chi' - \boldsymbol{e}_{z'} y' \sin\alpha), \end{aligned} \tag{29}$$

where

$$I_s = L[i(t)] = (I_0/s)(1 - \mathrm{e}^{-t_0 s}). \tag{30}$$

The Coulomb's gauge $\boldsymbol{\nabla} \cdot \boldsymbol{A}_{11} = 0$ in the coordinates o–xyz is transformed into

$$\boldsymbol{\nabla}' \cdot \boldsymbol{\mu}'_1 \boldsymbol{A}'_{11} = 0. \tag{31}$$

After applying the Laplace transform to Eq. (31), substituting it into Eq. (29) and applying the Fourier transform for the variables x', y', z' by the form of

$$F(u',v',w') = \int_{-\infty}^{+\infty}\int_{-\infty}^{+\infty}\int_{-\infty}^{+\infty} f(x',y',z')\,\mathrm{e}^{-\mathrm{j}\,(u'x'+v'y'+w'z')}\mathrm{d}x'\,\mathrm{d}y'\,\mathrm{d}z',$$

there are

$$-(u'^2+v'^2/\eta^2+w'^2)F'_{11x's} = \frac{\mu_1 I_s\cos\alpha}{\eta}\int_{-\infty}^{+\infty}\int_{-\infty}^{+\infty}\int_{-\infty}^{+\infty}\frac{y'}{\rho'}\delta(m')\delta(q')\mathrm{e}^{-\mathrm{j}\,(u'x'+v'y'+w'z')}\mathrm{d}x'\mathrm{d}y'\mathrm{d}z', \tag{32}$$

$$-(u'^2+v'^2/\eta^2+w'^2)F'_{11y's} = -\mu_1\eta I_s\int_{-\infty}^{+\infty}\int_{-\infty}^{+\infty}\int_{-\infty}^{+\infty}\frac{\chi'}{\rho'}\delta(m')\delta(q')\mathrm{e}^{-\mathrm{j}\,(u'x'+v'y'+w'z')}\mathrm{d}x'\mathrm{d}y'\mathrm{d}z', \tag{33}$$

$$-(u'^2+v'^2/\eta^2+w'^2)F'_{11z's} = \frac{\mu_1 I_s\sin\alpha}{\eta}\int_{-\infty}^{+\infty}\int_{-\infty}^{+\infty}\int_{-\infty}^{+\infty}\frac{y'}{\rho'}\delta(m')\delta(q')\mathrm{e}^{-\mathrm{j}\,(u'x'+v'y'+w'z')}\mathrm{d}x'\mathrm{d}y'\mathrm{d}z', \tag{34}$$

where $\boldsymbol{F}'_{11s}(u',v',w') = \boldsymbol{e}_{x'}F'_{11x's}+\boldsymbol{e}_{y'}F'_{11y's}+\boldsymbol{e}_{z'}F'_{11z's}$ is the Fourier transform of $\boldsymbol{A}'_{11s}(x',y',z') = \boldsymbol{e}_{x'}A'_{11x's}+\boldsymbol{e}_{y'}A'_{11y's}+\boldsymbol{e}_{z'}A'_{11z's}$. Equations (32) – (34) can be further simplified as

$$F'_{11x's} = \frac{\mathrm{j}\,2\mu_1 I_s\cot\alpha}{\eta(u'^2+v'^2/\eta^2+w'^2)}\int_{h-R\sin\alpha}^{h+R\sin\alpha}\mathrm{e}^{-\mathrm{j}\,w'p}\mathrm{e}^{-\mathrm{j}u'(p-h)\cot\alpha}\sin(v'n)\mathrm{d}p, \tag{35}$$

$$F'_{11y's} = \frac{2\mu_1\eta I_s}{u'^2+v'^2/\eta^2+w'^2}\int_{h-R\sin\alpha}^{h+R\sin\alpha}\mathrm{e}^{-\mathrm{j}w'p}\mathrm{e}^{-\mathrm{j}\,u'(p-h)\cot\alpha}\cos(v'n)\frac{p-h}{n\sin^2\alpha}\mathrm{d}p, \tag{36}$$

$$F'_{11z's} = \frac{\mathrm{j}\,2\mu_1 I_s}{\eta(u'^2+v'^2/\eta^2+w'^2)}\int_{h-R\sin\alpha}^{h+R\sin\alpha}\mathrm{e}^{-\mathrm{j}\,w'p}\mathrm{e}^{-\mathrm{j}u'(p-h)\cot\alpha}\sin(v'n)\mathrm{d}p, \tag{37}$$

where $n = \sqrt{R^2-(p-h)^2/\sin^2\alpha}$.

The following step is to apply the inverse Fourier transform

$$f(x',y',z') = \frac{1}{8\pi^3}\int_{-\infty}^{+\infty}\int_{-\infty}^{+\infty}\int_{-\infty}^{+\infty}F(u',v',w')\,\mathrm{e}^{\mathrm{j}\,(u'x'+v'y'+w'z')}\mathrm{d}u'\mathrm{d}v'\mathrm{d}w'$$

to Eqs. (35)–(37) for the variables u', v' and w' to obtain the magnetic vector potential $\boldsymbol{A}'_{11s}$.

Firstly, the inverse Fourier transform for the variable w' is applied to Eqs. (35)–(37).

Because the inverse Fourier transform of the function $\mathrm{e}^{-\mathrm{j}w'p}/k'^2+w'^2$ for the variable w' is $\mathrm{e}^{-k'|z'-p|}/k'$, i.e.,

$$\boldsymbol{F}_w^{-1}\left(\frac{\mathrm{e}^{-\mathrm{j}w'p}}{k'^2+w'^2}\right) = \frac{\exp(-k'|z'-p|)}{k'},$$

we can obtain the inverse Fourier transform $\boldsymbol{G}'_{11s}$ of $\boldsymbol{F}'_{11s}$ for the variables w':

$$G'_{11x's} = \frac{\mathrm{j}\,\mu_1 R I_s\cos\alpha}{\eta k'}\int_{-\pi/2}^{\pi/2} g'_1(u',z',\alpha,\theta)\sin(v'R\cos\theta)\cos\theta\mathrm{d}\theta, \tag{38}$$

$$G'_{11y's} = \frac{\mu_1\eta R I_s}{k'}\int_{-\pi/2}^{\pi/2} g'_1(u',z',\alpha,\theta)\cos(v'R\cos\theta)\sin\theta\,\mathrm{d}\theta, \tag{39}$$

$$G'_{11z's} = \frac{\mathrm{j}\,\mu_1 RI_s \sin\alpha}{\eta k'} \int_{-\pi/2}^{\pi/2} g'_1(u', z', \alpha, \theta) \sin(v' R\cos\theta)\cos\theta\,\mathrm{d}\theta, \tag{40}$$

where $k' = \sqrt{u'^2 + v'^2/\eta^2}$ and $g'_1(u', z', \alpha, \theta) = \mathrm{e}^{-k'|z'-h-R\sin\alpha\sin\theta|}\mathrm{e}^{-\mathrm{j}\,u' R\cos\alpha\sin\theta}$.

In the region $|z'-h| > R\sin\alpha$, there are

$$\int_{-\pi/2}^{\pi/2} g'_1(u', z', \alpha, \theta)\sin(v' R\cos\theta)\cos\theta\mathrm{d}\theta = \pi\frac{v'}{\psi'}\mathrm{I}_1(R\psi')\mathrm{e}^{\mp k'(z'-h)}$$

and

$$\int_{-\pi/2}^{\pi/2} g'_1(u', z', \alpha, \theta)\cos(v' R\cos\theta)\sin\theta\mathrm{d}\theta = \pi\frac{\mathrm{j}\,u'\cos\alpha \mp k'\sin\alpha}{\psi'}\mathrm{I}_1(R\psi')\mathrm{e}^{\mp k'(z'-h)},$$

where $\psi' = \sqrt{-u'^2\cos(2\alpha) - v'^2(1-\sin^2\alpha/\eta^2) \mp \mathrm{j}k'u'\sin(2\alpha)}$, $\mathrm{I}_1(x)$ is the first kind one-order modified Bessel function,[17] the negative sign (–) corresponds to the region $z'-h > R\sin\alpha$, while the positive sign (+) corresponds to the region $z'-h < -R\sin\alpha$.

According to the above two equations, by applying inverse Fourier transform for the variables u', v' to the expressions (38)–(40), the magnetic vector potential $\boldsymbol{A'}_{11s}$ can be obtained

$$A'_{11x's} = \frac{\mathrm{j}\,\mu_1 RI_s\cos\alpha}{4\eta\pi}\int_{-\infty}^{+\infty}\int_{-\infty}^{+\infty}\frac{v'}{k'\psi'}\mathrm{I}_1(R\psi')\,\mathrm{e}^{\mp k'(z'-h)+\mathrm{j}\,(u'x'+v'y')}\mathrm{d}u'\mathrm{d}v', \tag{41}$$

$$A'_{11y's} = \frac{-\mu_1\eta RI_s}{4\pi}\int_{-\infty}^{+\infty}\int_{-\infty}^{+\infty}\frac{\mathrm{j}\,u'\cos\alpha \mp k'\sin\alpha}{k'\psi'}\mathrm{I}_1(R\psi')\mathrm{e}^{\mp k'(z'-h)+\mathrm{j}\,(u'x'+v'y')}\mathrm{d}u'\mathrm{d}v', \tag{42}$$

$$A'_{11z's} = \frac{\mathrm{j}\,\mu_1 RI_s\sin\alpha}{4\eta\pi}\int_{-\infty}^{+\infty}\int_{-\infty}^{+\infty}\frac{v'}{k'\psi'}\mathrm{I}_1(R\psi')\mathrm{e}^{\mp k'(z'-h)+\mathrm{j}(u'x'+v'y')}\mathrm{d}u'\mathrm{d}v'. \tag{43}$$

We apply the inverse scale-transformation according to Eqs. (24) and (27), $u = u'$ and $v = v'/\eta$ to the expressions (41)–(43), then the expressions in the coordinate system o–xyz can be obtained as follows:

$$A_{11xs} = \frac{\mathrm{j}\,\mu_1\eta RI_s\cos\alpha}{4\pi}\int_{-\infty}^{+\infty}\int_{-\infty}^{+\infty}\frac{v}{\rho^2}\cdot\frac{\mathrm{I}_1(\rho R\psi_1)}{\psi_1}\,\mathrm{e}^{\mp\rho(z-h)+\mathrm{j}\,(ux+vy)}\mathrm{d}u\mathrm{d}v, \tag{44}$$

$$A_{11ys} = \frac{-\mu_1\eta RI_s}{4\pi}\int_{-\infty}^{+\infty}\int_{-\infty}^{+\infty}\frac{\mathrm{j}\,u\cos\alpha \mp \rho\sin\alpha}{\rho^2}\cdot\frac{\mathrm{I}_1(\rho R\psi_1)}{\psi_1}\,\mathrm{e}^{\mp\rho(z-h)+\mathrm{j}(ux+vy)}\mathrm{d}u\mathrm{d}v, \tag{45}$$

$$A_{11zs} = \frac{\mathrm{j}\,\mu_1\eta RI_s\sin\alpha}{4\pi}\int_{-\infty}^{+\infty}\int_{-\infty}^{+\infty}\frac{v}{\rho^2}\cdot\frac{\mathrm{I}_1(\rho R\psi_1)}{\psi_1}\mathrm{e}^{\mp\rho(z-h)+\mathrm{j}\,(ux+vy)}\mathrm{d}u\mathrm{d}v, \tag{46}$$

where $\rho = \sqrt{u^2+v^2}$ and $\psi_1 = \sqrt{-(u/\rho)^2\cos(2\alpha) - (v/\rho)^2(\eta^2-\sin^2\alpha) \mp \mathrm{j}\;u\sin(2\alpha)}$.

3.3. Determination of the unknown coefficients

The electric field strength $\boldsymbol{E}$ and the magnetic field intensity $\boldsymbol{H}$ at the adjacent surface $z = 0$ satisfy Eqs. (8) and (9), there are

$$A_{2xs}|_{z=0} - A_{1xs}|_{z=0} = 0, \tag{47}$$

$$A_{2ys}|_{z=0} - A_{1ys}|_{z=0} = 0, \tag{48}$$

$$\frac{\partial}{\partial x}\left(\frac{A_{2zs}}{\mu_2} - \frac{A_{1zs}}{\mu_1}\right)\bigg|_{z=0} = \frac{\partial}{\partial z}\left(\frac{A_{2xs}}{\mu_2} - \frac{A_{1xs}}{\mu_1}\right)\bigg|_{z=0}, \tag{49}$$

$$\frac{\partial}{\partial y}\left(\frac{A_{2zs}}{\mu_2} - \frac{A_{1zs}}{\mu_1}\right)\bigg|_{z=0} = \frac{\partial}{\partial z}\left(\frac{A_{2ys}}{\mu_2} - \frac{A_{1ys}}{\mu_1}\right)\bigg|_{z=0}. \tag{50}$$

According to the above four equations and two Coulomb's gauges $\boldsymbol{\nabla}\cdot\boldsymbol{A}_1 = 0$ and $\boldsymbol{\nabla}\cdot\boldsymbol{A}_2 = 0$, the coefficients $\boldsymbol{C}_{1s}$ and $\boldsymbol{C}_{2s}$ are solved, and $\boldsymbol{A}_{12s}$ and $\boldsymbol{A}_{2s}$ are obtained as follows:

$$A_{12xs} = \frac{\mu_1\eta RI_s}{2\pi}\int_0^{+\infty}\mathrm{d}\rho\int_{-\pi/2}^{+\pi/2}\mathrm{d}\beta\cdot\frac{\mathrm{I}_1(\rho R\psi_+)}{\psi_+}\cdot\frac{(\mu_1\lambda-\mu_2\rho)\cos\alpha+\mathrm{j}2\mu_2\rho\sin\beta\sin\alpha}{\mu_2\rho+\mu_1\lambda}$$

$$\times \cos\beta \sin(y\rho\cos\beta)\mathrm{e}^{-\rho(z+h)+\mathrm{j}\,x\rho\sin\beta}, \tag{51}$$

$$A_{12ys} = \frac{\mu_1\eta RI_s}{2\pi}\int_0^{+\infty}\mathrm{d}\rho\int_{-\pi/2}^{+\pi/2}\mathrm{d}\beta\cdot\frac{\mathrm{I}_1(\rho R\psi_+)}{\psi_+}\cdot\frac{[\mu_2\rho\cos(2\beta)+\mu_1\lambda]\sin\alpha+\mathrm{j}\,(\mu_2\rho+\mu_1\lambda)\sin\beta\cos\alpha}{\mu_2\rho+\mu_1\lambda}$$
$$\times\cos(y\rho\cos\beta)\mathrm{e}^{-\rho(z+h)+\mathrm{j}\,\rho x\sin\beta}, \tag{52}$$

$$A_{12zs} = \frac{-\mu_1\eta RI_s\sin\alpha}{2\pi}\int_0^{+\infty}\mathrm{d}\rho\int_{-\pi/2}^{+\pi/2}\mathrm{d}\beta\cdot\frac{\mathrm{I}_1(\rho R\psi_+)}{\psi_+}\cdot\cos\beta\sin(y\rho\cos\beta)\mathrm{e}^{\mp\rho(z-h)+\mathrm{j}\,x\rho\sin\beta}, \tag{53}$$

$$A_{2xs} = \frac{\mu_2\eta RI_s}{\pi}\int_0^{+\infty}\mathrm{d}\rho\int_{-\pi/2}^{+\pi/2}\mathrm{d}\beta\cdot\frac{\mathrm{I}_1(\rho R\psi_+)}{\psi_+}\cdot\frac{\mu_1}{\mu_2 k+\mu_1\lambda}$$
$$\times(\mathrm{j}\,\sin\beta\sin\alpha-\cos\alpha)\rho\cos\beta\sin(y\rho\cos\beta)\mathrm{e}^{\lambda z-kh+\mathrm{j}x\rho\sin\beta}, \tag{54}$$

$$A_{2ys} = \frac{-\mu_2\eta RI_s}{\pi}\int_0^{+\infty}\mathrm{d}\rho\int_{-\pi/2}^{+\pi/2}\mathrm{d}\beta\cdot\frac{\mathrm{I}_1(\rho R\psi_+)}{\psi_+}\cdot\frac{\mu_1}{\mu_2 k+\mu_1\lambda}$$
$$\times\rho\sin\beta(\sin\beta\sin\alpha+\mathrm{j}\,\cos\alpha)\cos(y\rho\cos\beta)\mathrm{e}^{\lambda z-\rho h+\mathrm{j}\,x\rho\sin\beta}, \tag{55}$$

$$A_{2zs} = 0, \tag{56}$$

where $\psi_+ = \sqrt{-\sin^2\beta\cos(2\alpha)-\cos^2\beta(\eta^2-\sin^2\alpha)+\mathrm{j}\,\sin\beta\sin(2\alpha)}$.

3.4. Expressions of the magnetic flux density and the eddy current density

According to $\boldsymbol{B}=\boldsymbol{\nabla}\times\boldsymbol{A}$ and $\boldsymbol{J}_{2s}=-\sigma s\boldsymbol{A}_{2s}$, and considering that $\mu_1=\mu_0$ and $\mu_2=\mu_0\mu_r$, the magnetic flux densities in the regions 1, 2 and the eddy current density in the region 2 are written as

$$B_{1xs} = \frac{\mu_0\eta RI_s}{2\pi}\int_0^{+\infty}\mathrm{d}\rho\int_{-\pi/2}^{+\pi/2}\mathrm{d}\beta\cdot\rho\sin\beta\cos(y\rho\cos\beta)\left[\frac{\lambda-\mu_r\rho}{\lambda+\mu_r\rho}\cdot(\sin\beta\sin\alpha+\mathrm{j}\cos\alpha)\right.$$
$$\left.\times\frac{\mathrm{I}_1(\rho R\psi_+)}{\psi_+}\mathrm{e}^{-\rho(z+h)}+(\sin\beta\sin\alpha\mp\mathrm{j}\cos\alpha)\cdot\frac{\mathrm{I}_1(\rho R\psi_\mp)}{\psi_\mp}\mathrm{e}^{-\rho|z-h|}\right]\cdot\mathrm{e}^{\mathrm{j}\,x\rho\sin\beta}, \tag{57}$$

$$B_{1ys} = \frac{\mu_0\eta RI_s}{2\pi}\int_0^{+\infty}\mathrm{d}\rho\int_{-\pi/2}^{+\pi/2}\mathrm{d}\beta\cdot\rho\cos\beta\sin(y\rho\cos\beta)\left[\frac{\lambda-\mu_r k}{\lambda+\mu_r k}(\mathrm{j}\,\sin\beta\sin\alpha-\cos\alpha)\right.$$
$$\left.\times\frac{\mathrm{I}_1(\rho R\psi_+)}{\psi_+}\mathrm{e}^{-\rho(z+h)}+(\mathrm{j}\,\sin\beta\sin\alpha-(\mp\cos\alpha))\frac{\mathrm{I}_1(\rho R\psi_\mp)}{\psi_\mp}\mathrm{e}^{-\rho|z-h|}\right]\cdot\mathrm{e}^{\mathrm{j}\,x\rho\sin\beta}, \tag{58}$$

$$B_{1zs} = \frac{\mu_0\eta RI_s}{2\pi}\int_0^{+\infty}\mathrm{d}\rho\int_{-\pi/2}^{+\pi/2}\mathrm{d}\beta\cdot\rho\cos(y\rho\cos\beta)\left[\frac{\lambda-\mu_r\rho}{\lambda+\mu_r\rho}\cdot(\mathrm{j}\,\sin\beta\sin\alpha-\cos\alpha)\right.$$
$$\left.\times\frac{\mathrm{I}_1(\rho R\psi_+)}{\psi_+}\mathrm{e}^{-\rho(z+h)}-(\mp\mathrm{j}\,\sin\beta\sin\alpha-\cos\alpha)\frac{\mathrm{I}_1(\rho R\psi_\mp)}{\psi_\mp}\mathrm{e}^{-\rho|z-h|}\right]\mathrm{e}^{\mathrm{j}\,x\rho\sin\beta}, \tag{59}$$

where $\psi_\mp = \sqrt{-\sin^2\beta\cos(2\alpha)-\cos^2\beta(\eta^2-\sin^2\alpha)\mp\mathrm{j}\,\sin\beta\sin(2\alpha)}$.

$$B_{2xs} = \frac{\mu\eta RI_s}{\pi}\int_0^{+\infty}\mathrm{d}\rho\int_{-\pi/2}^{+\pi/2}\mathrm{d}\beta\cdot\rho\cos(y\rho\cos\beta)\sin\beta(\sin\beta\sin\alpha+\mathrm{j}\cos\alpha)$$
$$\times\frac{\lambda}{\mu_r\rho+\lambda}\cdot\frac{\mathrm{I}_1(\rho R\psi_+)}{\psi_+}\mathrm{e}^{\lambda z-\rho h+\mathrm{j}\,x\rho\sin\beta}, \tag{60}$$

$$B_{2ys} = \frac{\mu\eta RI_s}{\pi}\int_0^{+\infty}\mathrm{d}\rho\int_{-\pi/2}^{+\pi/2}\mathrm{d}\beta\cdot\rho\cos\beta\sin(y\rho\cos\beta)(\mathrm{j}\,\sin\beta\sin\alpha-\cos\alpha)$$
$$\times\frac{\lambda}{\mu_r\rho+\lambda}\cdot\frac{\mathrm{I}_1(\rho R\psi_+)}{\psi_+}\mathrm{e}^{\lambda z-\rho h+\mathrm{j}\,x\rho\sin\beta}, \tag{61}$$

$$B_{2zs} = \frac{\mu\eta RI_s}{\pi}\int_0^{+\infty}\mathrm{d}\rho\int_{-\pi/2}^{+\pi/2}\mathrm{d}\beta\cdot\frac{\rho^2}{\mu_r\rho+\lambda}\cos(y\rho\cos\beta)(\cos\alpha-\mathrm{j}\,\sin\beta\sin\alpha)\frac{\mathrm{I}_1(\rho R\psi_+)}{\psi_+}\mathrm{e}^{\lambda z-\rho h+\mathrm{j}\,x\rho\sin\beta}, \tag{62}$$

$$J_{2xs} = \frac{\mu\sigma\eta RsI_s}{\pi}\int_0^{+\infty}\mathrm{d}\rho\int_{-\pi/2}^{+\pi/2}\mathrm{d}\beta\cdot\cos\beta\sin(y\rho\cos\beta)(\cos\alpha-\mathrm{j}\sin\beta\sin\alpha)$$

$$\times \frac{\rho}{\mu_r\rho+\lambda}\cdot\frac{\mathrm{I}_1(\rho R\psi_+)}{\psi_+}\mathrm{e}^{\lambda z-\rho h+\mathrm{j}\,x\rho\sin\beta}, \tag{63}$$

$$J_{2ys} = \frac{\mu\sigma\eta RsI_s}{\pi}\int_0^{+\infty}\mathrm{d}\rho\int_{-\pi/2}^{+\pi/2}\mathrm{d}\beta\cdot\cos(y\rho\cos\beta)\sin\beta(\sin\beta\sin\alpha+\mathrm{j}\,\cos\alpha)$$
$$\times \frac{\rho}{\mu_r\rho+\lambda}\cdot\frac{\mathrm{I}_1(\rho R\psi_+)}{\psi_+}\mathrm{e}^{\lambda z-\rho h+\mathrm{j}\,x\rho\sin\beta}, \tag{64}$$

$$J_{2zs} = 0. \tag{65}$$

3.5. Field distributions in the time domain

Applying the inverse Laplace transform to the expressions (57)–(59) and (63)–(65), the expressions of electromagnetic field distributions in the time domain can be obtained as follows:

$$B_{1x} = \frac{\mu_0\eta R}{2\pi}\int_0^{+\infty}\mathrm{d}\rho\int_{-\pi/2}^{+\pi/2}\mathrm{d}\beta\cdot\rho\sin\beta\cos(y\rho\cos\beta)\Big[i(t)(\sin\beta\sin\alpha\mp\mathrm{j}\cos\alpha)$$
$$\times\frac{\mathrm{I}_1(\rho R\psi_\mp)}{\psi_\mp}\cdot\mathrm{e}^{-\rho|z-h|}-i(t)*\Theta(t)\ \cdot(\sin\beta\sin\alpha+\mathrm{j}\cos\alpha)\cdot\frac{\mathrm{I}_1(\rho R\psi_+)}{\psi_+}\mathrm{e}^{-\rho(z+h)}\Big]\cdot\mathrm{e}^{\mathrm{j}\,x\rho\sin\beta}, \tag{66}$$

$$B_{1y} = \frac{\mathrm{j}\,\mu_0\eta R}{2\pi}\int_0^{+\infty}\mathrm{d}\rho\int_{-\pi/2}^{+\pi/2}\mathrm{d}\beta\cdot\rho\cos\beta\sin(y\rho\cos\beta)\Big[i(t)(\sin\beta\sin\alpha\mp\mathrm{j}\cos\alpha)$$
$$\times\frac{\mathrm{I}_1(\rho R\psi_\mp)}{\psi_\mp}\cdot\mathrm{e}^{-\rho|z-h|}-i(t)*\Theta(t)\cdot(\sin\beta\sin\alpha+\mathrm{j}\cos\alpha)\frac{\mathrm{I}_1(\rho R\psi_+)}{\psi_+}\mathrm{e}^{-\rho(z+h)}\Big]\mathrm{e}^{\mathrm{j}\,x\rho\sin\beta}, \tag{67}$$

$$B_{1z} = \frac{\mu_0\eta R}{2\pi}\int_0^{+\infty}\mathrm{d}\rho\int_{-\pi/2}^{+\pi/2}\mathrm{d}\beta\cdot\rho\cos(y\rho\cos\beta)\Big\{i(t)[\cos\alpha-\mathrm{j}(\mp\sin\beta\sin\alpha)]$$
$$\times\frac{\mathrm{I}_1(\rho R\psi_\mp)}{\psi_\mp}\mathrm{e}^{-\rho|z-h|}+i(t)*\Theta(t)\cdot(\cos\alpha-\mathrm{j}\,\sin\beta\sin\alpha)\frac{\mathrm{I}_1(\rho R\psi_+)}{\psi_+}\mathrm{e}^{-\rho(z+h)}\Big\}\cdot\mathrm{e}^{\mathrm{j}\,x\rho\sin\beta}, \tag{68}$$

where

$$\Theta(t) = -\delta(t)+\frac{2\mu_r\rho}{\sqrt{\pi\mu\sigma t}}\mathrm{e}^{-\rho^2t/\mu\sigma}-\frac{2\mu_r\rho^2}{\mu_0\sigma}\mathrm{e}^{(\mu_r^2-1)\rho^2t/\mu\sigma}\mathrm{erfc}\Big(\rho\sqrt{\frac{\mu_r t}{\mu_0\sigma}}\Big),$$

erfc( ) is the complementary error function,

$$\mathrm{erfc}(\vartheta) = 1-\mathrm{erf}(\vartheta) = \frac{2}{\sqrt{\pi}}\int_\vartheta^\infty \mathrm{e}^{-y^2}\mathrm{d}y;$$

$f_1(t)*f_2(t)$ is the inverse Laplace transform of $F_1(s)\cdot F_2(s)$, $f_1(t)*f_2(t)=\int_0^\infty f_1(\tau)f_2(t-\tau)\mathrm{d}\tau$. When $z<0$,

$$J_{2x} = \frac{\eta R\mu\sigma z}{2\pi}\int_0^{+\infty}\mathrm{d}\rho\int_{-\pi/2}^{+\pi/2}\mathrm{d}\beta\cdot i'(t)*\Gamma(t)\cdot\rho\cos\beta\sin(y\rho\cos\beta)$$
$$\times(\mathrm{j}\,\sin\beta\sin\alpha-\cos\alpha)\frac{\mathrm{I}_1(\rho R\psi_+)}{\psi_+}\mathrm{e}^{-\rho h+\mathrm{j}x\rho\sin\beta}, \tag{69}$$

$$J_{2y} = \frac{-\eta R\mu\sigma z}{2\pi}\int_0^{+\infty}\mathrm{d}\rho\int_{-\pi/2}^{+\pi/2}\mathrm{d}\beta\cdot i'(t)*\Gamma(t)\cdot\rho\sin\beta\cos(y\rho\cos\beta)$$
$$\times(\sin\beta\sin\alpha+\mathrm{j}\,\cos\alpha)\cdot\frac{\mathrm{I}_1(\rho R\psi_+)}{\psi_+}\cdot\mathrm{e}^{-\rho h+\mathrm{j}\,x\rho\sin\beta}, \tag{70}$$

$$J_{2z} = 0, \tag{71}$$

where $i'(t)=\mathrm{d}i(t)/\mathrm{d}t$ and

$$\Gamma(t) = \Big\{\mathrm{e}^{-\rho^2t/\mu\sigma}\Big[\frac{1}{\sqrt{\pi t}}-\rho\sqrt{\frac{\mu_r}{\mu_0\sigma}}\mathrm{e}^{\mu_r\rho^2t/\mu_0\sigma}\mathrm{erfc}\Big(\rho\sqrt{\frac{\mu_r t}{\mu_0\sigma}}\Big)\Big]\Big\}*\Big\{\frac{\mathrm{e}^{-\rho^2t/\mu\sigma-z^2\mu\sigma/4t}}{\sqrt{\pi t^3}}\Big\}.$$

When $z=0$,

$$J_{2x} = \frac{\eta RI_0\mu\sigma}{\pi}\int_0^{+\infty}\mathrm{d}\rho\int_{-\pi/2}^{+\pi/2}\mathrm{d}\beta\cdot i'(t)*\Gamma_0(t)\cdot\rho\cos\beta\sin(y\rho\cos\beta)$$

$$\times(\cos\alpha-\mathrm{j}\,\sin\beta\sin\alpha)\frac{\mathrm{I}_1(\rho R\psi_+)}{\psi_+}\cdot\mathrm{e}^{-\rho h+\mathrm{j}x\rho\sin\beta}, \tag{72}$$

$$J_{2y}=\frac{\eta R I_0\mu\sigma}{\pi}\int_0^{+\infty}\mathrm{d}\rho\int_{-\pi/2}^{+\pi/2}\mathrm{d}\beta\cdot i'(t)*\Gamma_0(t)\cdot\rho\cos(y\rho\cos\beta)$$
$$\times\sin\beta(\sin\beta\sin\alpha+\mathrm{j}\,\cos\alpha)\frac{\mathrm{I}_1(\rho R\psi_+)}{\psi_+}\cdot\mathrm{e}^{-\rho h+\mathrm{j}\,x\rho\sin\beta}, \tag{73}$$

$$J_{2z}=0, \tag{74}$$

where

$$\Gamma_0(t)=\mathrm{e}^{-\rho^2 t/\mu\sigma}\left[\frac{1}{\sqrt{\pi\mu\sigma t}}-\frac{\rho}{\mu_0\sigma}\mathrm{e}^{\rho^2 t\mu_r/\mu_0\sigma}\mathrm{erfc}(\rho\sqrt{\mu_r t/(\mu_0\sigma)})\right].$$

3.6. Field distributions of transient pulsed eddy current

Substituting the expression of excitation current $i(t)$ into the expressions (69)–(74), electromagnetic field distributions in the time domain excited by the pulsed current can be obtained, and some expressions can be simplified by

$$i'(t)*\Gamma(t)=I_0\cdot\left\{\mathrm{e}^{-\rho^2 t/\mu\sigma}\left[\frac{1}{\sqrt{\pi t}}-\rho\sqrt{\frac{\mu_r}{\mu_0\sigma}}\,\mathrm{e}^{\rho^2 t\mu_r/\mu_0\sigma}\mathrm{erfc}\left(\rho\sqrt{\frac{\mu_r t}{\mu_0\sigma}}\right)\right]\right\}$$
$$*\left[u(t-t_0)\cdot\frac{\mathrm{e}^{-\rho^2(t-t_0)/\mu\sigma-z^2\mu\sigma/4(t-t_0)}}{\sqrt{\pi(t-t_0)^3}}-\frac{\mathrm{e}^{-\rho^2 t/\mu\sigma-z^2\mu\sigma/4t}}{\sqrt{\pi t^3}}\right], \tag{75}$$

$$i'(t)*\Gamma_0(t)=I_0\cdot\left\{u(t)\cdot\left[\frac{1}{\sqrt{\pi\mu\sigma t}}-\frac{\rho}{\mu_0\sigma}\mathrm{e}^{\rho^2 t\mu_r/\mu_0\sigma}\mathrm{erfc}\left(\rho\sqrt{\frac{\mu_r t}{\mu_0\sigma}}\right)\right]\cdot\mathrm{e}^{-\rho^2 t/\mu\sigma}-u(t-t_0)\right.$$
$$\left.\times\left[\frac{1}{\sqrt{\pi\mu\sigma(t-t_0)}}-\frac{\rho}{\mu_0\sigma}\mathrm{e}^{\rho^2(t-t_0)\mu_r^2/\mu\sigma}\mathrm{erfc}\left(\rho\sqrt{\frac{\mu_r(t-t_0)}{\mu_0\sigma}}\right)\right]\cdot\mathrm{e}^{-\rho^2(t-t_0)/\mu\sigma}\right\}. \tag{76}$$

4. Figure-8-shaped elliptical coil and validation of analytical solutions

Based on the above analytical solutions of transient pulsed eddy current field generated by a single oblique elliptical coil, and according to the linear superposition principle in the homogeneous isotropic linear medium, electromagnetic fields produced by multi-turn coils can be obtained by integral.

In the following, we will calculate and analyse the field distributions generated by the figure-8-shaped elliptical concentrative coil, which is composed of two identical geometric elliptical single-turn loops C_1 and C_2 on the symmetry of plane yoz, as shown in Fig. 3. The angle between two loops $2\beta=180^\circ-2\alpha$ is called the spread angle of figure-8-shaped elliptical concentrative coil. The lift-off height $h_1=h-R\sin\alpha$.

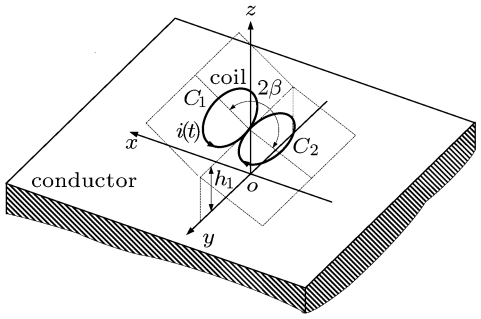


Fig. 3. Model of figure-8-shaped elliptical concentrative coil.

Assume that the half-infinite conductor is aluminum, whose relative magnetic permeability $\mu_r=1$ and conductivity $\sigma=37\times10^6$ S/m. The radius of transverse axis is $R=5$ mm. $h_1=1$ mm, $I_0=1$ A and $t_0=1$ ms.

For the measurement of transient pulsed eddy current field is difficult for us, here analytical solutions will be compared with numerical solutions.

4.1. Comparisons of analytical solutions and numerical solutions

Assume that the spread angle $2\beta = 120°$ and η=1.4. Let $t_{0+} = 1 \times 10^{-8}$ s. The Ansoft software is applied to our calculation. The current loop is modeled by a conducting loop whose section is 0.01 mm×0.01 mm, and the half-infinite conductor is modeled by a conductor of 100 mm(length)×100 mm(width)×20 mm(thickness). The magnetic flux densities at some points when $t = 0.9$ ms are listed in Table 1.

We can see from Table 1 that the analytical solutions are basically the same as the numerical solutions. The differences of analytical and numerical methods are: compared with the numerical method, analytical method can obtain the solutions quicker and more accurate. For example, from the expression (67), we know that $B_{1y} = 0$ when $y = 0$, while numerical solutions are close to zero, but not zero.

Table 1. Magnetic flux densities $\boldsymbol{B}$ ($\times 10^{-5}$ T).

No.	$\left(\frac{x}{R}, \frac{y}{R}, \frac{z}{R}\right)$	(B_x, B_y, B_z)	
		analytical solutions	numerical solutions
1	(0.2, 0, 0)	(14.60, 0, 19.00)	(15.37, –0.11, 19.38)
2	(0.4, 0, 0)	(3.47, 0, 15.70)	(3.84, –0.00, 16.05)
3	(0.6, 0, 0)	(–0.29, 0, 11.99)	(0.15, –0.03, 12.30)
4	(0.8, 0, 0)	(–1.87, 0, 9.47)	(–1.49, –0.02, 9.82)
5	(1.0, 0, 0)	(–2.72, 0, 7.65)	(–2.40, –0.02, 8.03)
6	(1.2, 0, 0)	(–3.22, 0, 6.20)	(–2.96, –0.02, 6.59)
7	(1.4, 0, 0)	(–3.48, 0, 4.92)	(–3.30, –0.01, 5.31)
8	(1.6, 0, 0)	(–3.55, 0, 3.71)	(–3.43, –0.01, 4.10)
9	(1.8, 0, 0)	(–3.39, 0, 2.64)	(–3.34, –0.01, 2.98)
10	(2.0, 0, 0)	(–3.06, 0, 1.71)	(–3.03, –0.01, 2.01)

4.2. Eddy current distributions on the surface of conductor

Assume the spread angle $2\beta = 120°$, $\eta = 0.6$ and 1.4, $t = 0.01$ ms. The eddy current distributions on the surface of conductor, $z = 0$, are shown in Figs. 4 and 5.

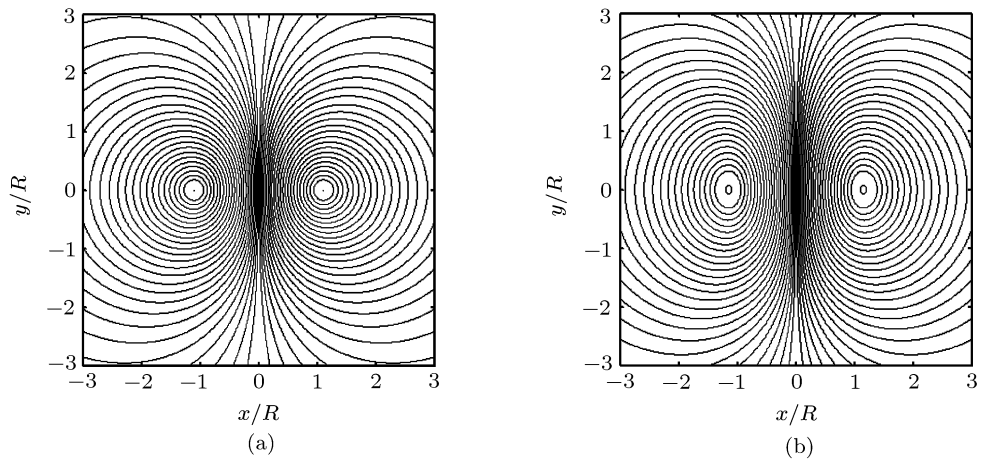


Fig. 4. Eddy current distributions by analytical method when (a) $\eta = 0.6$ and (b) $\eta = 1.4$.

From Figs. 4 and 5, we can see that eddy current distributions by analytical method and Ansoft software are consistent with each other. The eddy currents are focused on the conductor under the geometric symmetric

centre of concentrative coil, where eddy currents have a good concentrative effect.

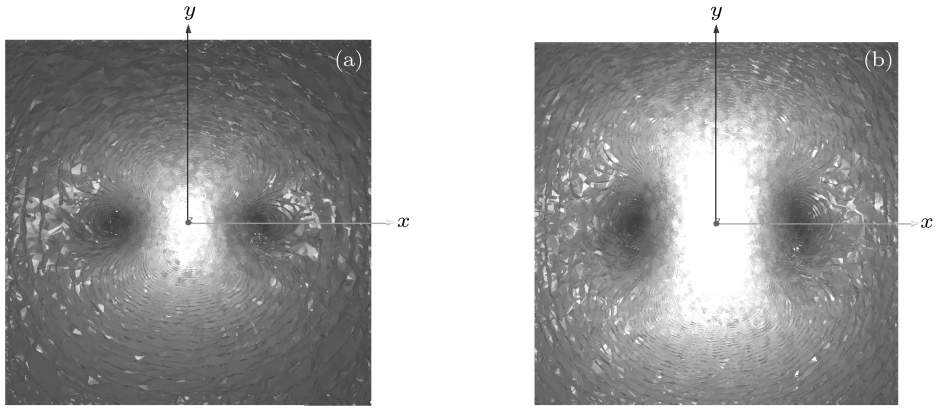


Fig. 5. Eddy current distributions by using Ansoft software when (a) $\eta = 0.6$ and (b) $\eta = 1.4$.

5. Calculations of electromagnetic field due to a figure-8-shaped coil

All the parameters in the following calculations are the same as those in Section 4.

5.1. Time domain responses of eddy current density

Figure 6 shows the change of eddy current density J_y at the point $P_0(0,0,0)$ when $2\beta = 120°$ and $\eta = 1.4$.

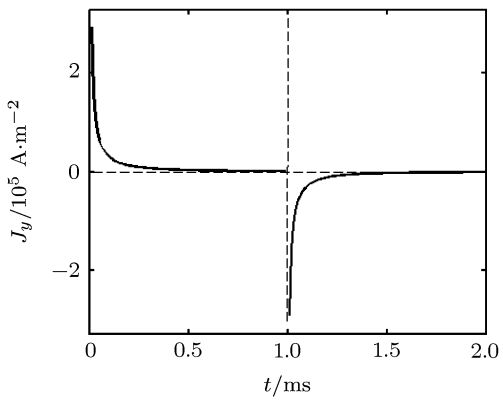


Fig. 6. Eddy current densities J_y versus time t.

The eddy current densities J_y have the large peak values at the rising and falling edges of the excitation current, then decrease to zero quickly.

5.2. Time domain response of magnetic flux density

Figure 7 shows the changes of magnetic flux density component in direction z, B_z, with time t at three points $P_1(0.4R,0,0)$, $P_2(R,0,0)$ and $P_3(2R,0,0)$ when $2\beta = 120°$ and $\eta = 1.4$.

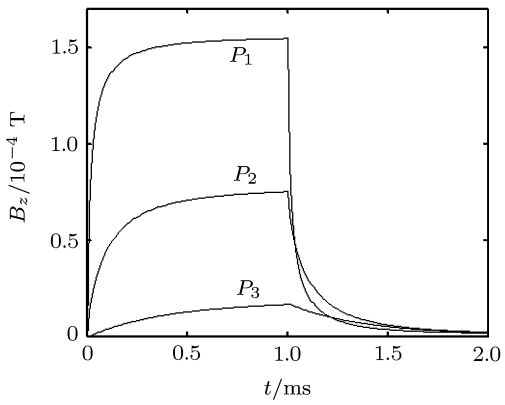


Fig. 7. Magnetic flux densities B_z versus time t.

The magnetic flux densities B_z at these three points raise to the steady-state values from zero quickly at the rising edge of the excitation current, and decrease to zero quickly at the falling edge of the excitation current. The closer the point is to eddy current centre, the more like square-wave of time-varying curve of magnetic flux density B_z on the point. In the eddy current testing, the magnetic flux densities are usually measured for obtaining the information of defects in the conductor.

5.3. Effects of scale factor of ellipse on the concentrative characteristics

Figure 8 shows the eddy current densities J_y in the direction x and y at the point $P_0(0,0,0)$ when $2\beta = 120°$, $t = 0.01$ ms and the scale factor of ellipse $\eta = 0.6$, 0.8, 1.0, 1.2, and 1.4, respectively, corresponding to the curves a–e.

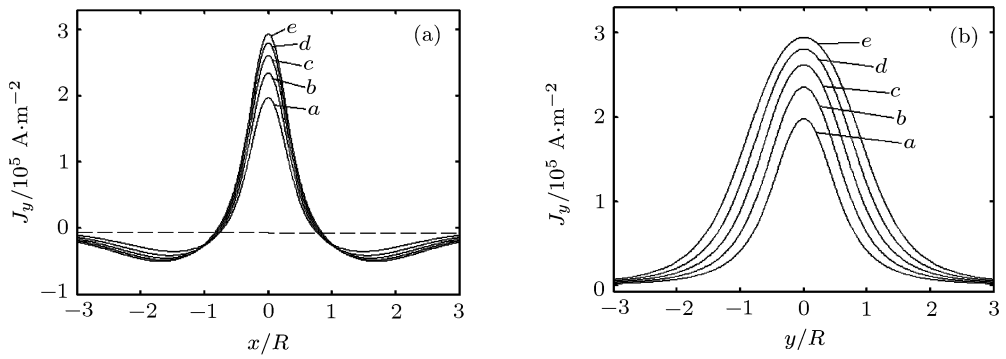


Fig. 8. Eddy current densities of different scale factors η: (a) along x axis; (b) along y axis.

The greater the scale factor of ellipse η is, the higher the eddy current density is and the wider the concentrative area of eddy current along y axis is.

5.4. Effect of spread angle on the concentrative characteristic

Figure 9 shows the eddy current densities along x axis and y axis generated by the figure-8-shaped elliptical coils with different spread angles at the point $P_0(0,0,0)$ when $\eta = 1.4$ and $t = 0.01$ ms, where the curves a–d are corresponding to $2\beta = 0°$, 60°, 120°, and 180°, respectively.

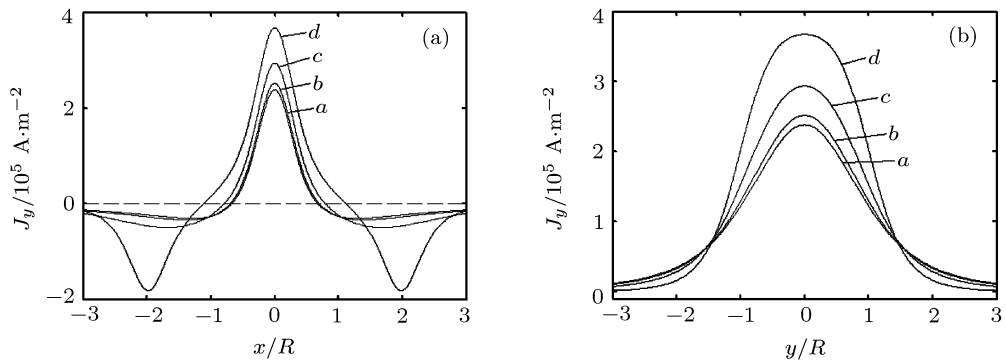


Fig. 9. Eddy current densities of different spread angles: (a) along x axis; (b) along y axis.

The maximum magnitude of eddy current density increases when spread angle 2β increases, while there are two reverse concentrative area on both sides of x axis when $2\beta = 180°$ besides the central concentrative area.

6. Conclusions

In this paper, the analytical solutions of transient pulsed eddy current problem due to elliptical concentrative coil over the half-infinite plane conductor have been derived. Through calculating the electromagnetic fields produced by a figure-8-shaped elliptical coil, we have the following conclusions: i) eddy currents are focused on the conductor under the geometric symmetric centre of figure-8-shaped concentrative coil, where eddy currents have the good concentrative characteristics; ii) at the rising edge of the excitation current, the eddy current

density has a large peak value, then decreases to zero quickly, and the magnetic flux density also raises to the steady-state value from zero quickly; while at the falling edge, the eddy current density has a reverse large peak value, then decreases to zero quickly, and the magnetic flux density also decreases to zero quickly. The closer the point is to eddy current centre, the more like square-wave of time-varying curve of magnetic flux density on the point; iii) the greater the scale factor of ellipse η is, the higher the eddy current density is and the wider the concentrative area of eddy current along y axis is; iv) the maximum magnitude of eddy current densities increases when spread angle 2β increases. When $2\beta = 180°$, there are two additional reverse concentrative areas on both sides of x axis.

The research on the analytical solutions of transient pulsed eddy current problem due to elliptical concentrative coils plays an important role in improving the measurement sensitivity and designing new magnetic probe in the applications of biomedical functional magnetic stimulation and nondestructive testing, etc.

References

[1] Iramina K, Maeno T, Nonaka Y and Ueno S 2003 *J. Appl. Phys.* **93** 6718

[2] Ueno S, Tashiro T and Harada K 1988 *J. Appl. Phys.* **64** 5862

[3] Zhang J Y and Lei Y Z 2007 *Nondestructive Testing* **29** 57

[4] Ren C, Tarjan P P and Popovic D B 1995 *IEEE Trans. Biomed. Eng.* **42** 918

[5] Hsu K H and Durand D M 2001 *IEEE Trans. Biomed. Eng.* **48** 1162

[6] Salinas F S, Lancaster J L and Fox P T 2009 *Phys. Med. Biol.* **54** 3631

[7] Lin V W, Hsiao I N and Dhaka V 2000 *IEEE Trans. Biomed. Eng.* **47** 600

[8] Ruohonen J and Ilmoniemi R J 1998 *Med. Biol. Eng. Comput.* **36** 297

[9] Pu L N , Yin T, An H, Li S and Liu Z P 2008 *Journal of Biomedical Engineering Research* **27** 74

[10] Ho S L, Xu G Z, Fu W N, Yang Q X, Hou H J and Yan W L 2009 *IEEE Trans. Magn.* **45** 4849

[11] Tsaknakis H J and Kriezis E E 1982 *IEEE Trans. Geosci. Remote Sensing* **20** 122

[12] Tsaknakis H J and Kriezis E E 1985 *IEEE Trans. Geosci. Remote Sensing* **23** 834

[13] Xie L and Lei Y Z 2007 *Chin. Phys.* **16** 2523

[14] Thomson W T 1960 *Laplace Transformation* (Englewood Cliffs: Prentice-Hall INC.) p. 245

[15] Campbell G A and Foster R M 1948 *Fourier Integrals for Practical Application* (New York: Van Nostrand Co.) pp. 56, 57

[16] Li Y L and Huang J Y 2005 *Chin. Phys.* **14** 646

[17] Liu S S and Liu S D 2002 *Special Functions* (2nd edn.) (Beijing: China Meteorological Press) p. 434